AIAA JOURNAL
Vol. 47, No. 8, August 2009

Validation of a Time- and Frequency-Domain Grazing Flow Acoustic Liner Model

Markus O. Burak*
Chalmers University of Technology, SE-412 96 Gothenburg, Sweden
Mattias Billson†
Volvo Aero Corporation, SE-461 81 Trollhättan, Sweden
Lars-Erik Eriksson‡
Chalmers University of Technology, SE-412 96 Gothenburg, Sweden
and
Stéphane Baralon§
Volvo Aero Corporation, SE-461 81 Trollhättan, Sweden

DOI: 10.2514/1.40870

In today's aeroengines, acoustic liners are extensively used to suppress noise. To optimize their placement and tuning, there is a need for acoustic liner models capturing their effect. Traditionally, the presence of a mean flow has been accounted for through the Ingard or later the generalization in form of the Myers boundary condition. This paper shows that a direct use of nominal impedance for the acoustic liner is justified if the mean flow is properly accounted for by the flow equations. An accurate assessment of the acoustic liner in the presence of grazing flows can be obtained without using an acoustic liner model accounting for the flow, for example, the Myers boundary condition. Validations have been made for both time and frequency-domain solvers using large-eddy simulations and linearized Navier–Stokes equations.

Nomenclature

C_p	=	specific heat at constant pressure
C_R, C_I	=	Smagorinsky model coefficients
c	=	speed of sound
e	=	energy
$\mathcal{F}_j$	=	Cartesian components of flux vector
f	=	frequency
M	=	Mach number
Pr	=	Prandtl number
p	=	pressure
$\mathbf{Q}$	=	state vector
R	=	liner resistance
R_0, X_-, X_+	=	parameters of the three-parameter impedance model
S_{ij}	=	strain rate tensor
T	=	temperature
t	=	time
u_i	=	Cartesian components of velocity vector
v_n	=	wall normal velocity
X	=	liner reactance
x_i	=	Cartesian coordinate vector component
Z	=	acoustic impedance
γ	=	gas constant
Δ	=	filter width
δ_{ij}	=	Kronecker delta
μ	=	dynamic viscosity
ρ	=	density
σ_{ij}	=	viscous stress tensor
τ_{ij}	=	subgrid-scale stress tensor

Subscripts

t	=	turbulent quantity
0	=	total condition
∞	=	ambient condition

Superscripts

SGS	=	subgrid scale
-	=	spatially filtered quantity or time-averaged quantity
~	=	spatially Favre-filtered quantity
^	=	frequency-domain quantity

Presented as Paper 2929 at the 14th AIAA/CEAS Aeroacoustics Conference, Vancouver, Canada, 5–7 May 2008; received 8 September 2008; revision received 19 February 2009; accepted for publication 6 March 2009.

*Ph.D. Student, Division of Fluid Dynamics, Department of Applied Mechanics.
†Aeroacoustic Specialist, Product Development, Center of Excellence Aerothermodynamics.
‡Professor, Division of Fluid Dynamics, Department of Applied Mechanics.
§Aeroacoustic Specialist, Product Development, Center of Excellence Aerothermodynamics.

I. Introduction

HARSHER regulations on noise have positioned acoustics as a key element in the development of novel aeroengines. With the increased size of aeroengines, fan noise has become one of the major noise sources. To reduce this noise, acoustic liners have been used extensively throughout the duct system. This has emphasized the need for models that give the correct assessment of the acoustic liners. A liner can be characterized by its impedance, which is a frequency-dependent complex number for which the real and imaginary parts relate to the resistance and reactance, respectively. The resistance is related to the dissipation of energy when the sound wave impinges on the liner surface, and the reactance is related to the phase shift of the reflected wave. The frequency dependence of the impedance is determined by the type of liner. There are a variety of different liners, for example, Helmholtz resonator, tubular liner, bulk liner, and perforated plate, to mention a few. Helmholtz resonators have a high absorption within a narrow frequency band and are very efficient as tonal absorbents, whereas, for example, bulk liners have a

lower efficiency but for a wider frequency range and thus are more beneficial for broadband attenuation.

Almost all environments in which acoustic liners are considered in aeroengines involve a mean flow with a boundary layer outside the lined wall. The boundary layer refracts the sound waves and affects the effective liner impedance. Traditionally, this has been compensated for through the Ingard [1] or later the generalization in form of the Myers [2] boundary condition. If the boundary layer is fully resolved, this gives a zero modification of the impedance and the nominal impedance of the liner is used. The nominal impedance refers to the impedance of the acoustic liner in a stagnant surrounding. A problem with convective impedance boundary conditions is that they may generate spurious unstable solutions of Kelvin–Helmholtz type, first found by Tester [3] and later by, for example, Rienstra [4]. A general proof of the existence of such instabilities was given by Tam and Auriault [5]. Different convective impedance boundary conditions have been developed for plug flows. For example, Özyörük and Long [6] proposed a convective-modified method via z transformation, and Fung and Ju [7,8] used the reflection coefficient instead of the impedance as the boundary condition. The convective impedance boundary conditions have been extended to sheared flows giving less numerical instabilities, for example, Özyörük et al. [9] and Li and Thiele [10]. Li et al. [11] proposed a Myers-based time-domain formulation as an extension to the work by Tam and Auriault [5], which is reported to be numerically stable.

If the boundary-condition formulation could be separated from the mean-flow condition, it would not only simplify the boundary condition but also simplify the design process when optimizing liner placement. This paper will show that the nominal impedance may be used directly with a Navier–Stokes-based wave operator, for example, large-eddy simulation (LES) [12] or linearized Navier–Stokes equations (LNSE) [13]. The wave operator, LES or LNSE, takes care of the mean-flow effects on the wall impedance. There is then no need for the use of the Myers type of boundary conditions. By resolving the boundary layer, it is logical that the nominal impedance of the liner should be used as a boundary condition. A similar approach was suggested by Zheng and Zhuang [14], where the linearized Euler equations were solved using an analytical description of the sheared mean flow. However, resolving the boundary layers may be exhaustive in terms of computational effort. The question is how well resolved the near wall region has to be to still capture the mean-flow effects on the liner efficiency. By only resolving the near wall region down to the logarithmic layer, wall functions can be used to obtain the correct wall friction. This considerably reduces the computational cost and is also a common method in aerodynamic simulations. It is most often also the only option available when considering high Reynolds number flow. The partly resolved boundary layer, together with the characterization of the lined wall by its nominal impedance, is believed by the authors to be sufficient for accurate description of the acoustic liner. This is supported by results based on time-domain LES and frequency-domain LNSE simulations on a benchmark test case [15], which will be presented next.

II. Overview of the Present Study

The test case considered in this paper is the grazing incidence tube (GIT) at NASA Langley Research Center [16]. The test section consists of a $0.8128 \times 0.0508 \times 0.0508$ m duct with a centralized lined section of 0.4064 m (see Fig. 1). The liner used in the experiment is a ceramic tubular liner (CT57). Two test cases have been considered in the numerical study. First is the case in which plane waves are introduced without mean flow inside the duct, hereafter referred to as case I. Second is the case in which plane waves are introduced together with a mean flow of average Mach 0.335 over the liner, hereafter referred to as case II. Experimental data, nominal impedance of the liner, as well as flow conditions were given by Jones et al. [15] (see Tables 1 and 2). In both case I and case II, six incoming frequencies ranging from 500 to 3000 Hz were studied.

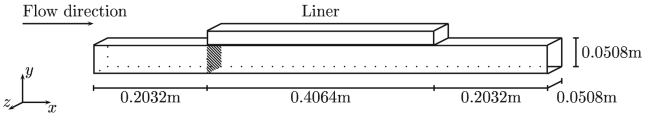

Fig. 1 Grazing incidence tube test section.

III. Governing Equations

A. Large-Eddy Simulation Method

The equations solved are the spatially Favre-filtered continuity, momentum, and energy equations:

$$\frac{\partial \mathbf{Q}}{\partial t} + \frac{\partial \mathcal{F}_j}{\partial x_j} = 0 \tag{1}$$

where

$$\mathbf{Q} = \begin{bmatrix} \bar{\rho} \\ \bar{\rho}\tilde{u}_i \\ \bar{\rho}\tilde{e}_0 \end{bmatrix} \tag{2}$$

and

$$\mathcal{F}_j = \begin{bmatrix} \bar{\rho}\tilde{u}_j \\ \bar{\rho}\tilde{u}_i\tilde{u}_j + \bar{p}\delta_{ij} - \bar{\sigma}_{ij} - \tau_{ij} \\ \bar{\rho}\tilde{e}_0\tilde{u}_j + \bar{p}\tilde{u}_j - C_p\left[\left(\frac{\mu}{Pr} + \frac{\mu_t}{Pr_t}\right)\frac{\partial \tilde{T}}{\partial x_j}\right] - \tilde{u}_i(\bar{\sigma}_{ij} + \tau_{ij}) \end{bmatrix} \tag{3}$$

where the Favre-filtered viscous stress tensor is given by

$$\bar{\sigma}_{ij} = \mu(2\tilde{S}_{ij} - \tfrac{2}{3}\tilde{S}_{mm}\delta_{ij}) \tag{4}$$

The subgrid-scale model used for the LES method is the Smagorinsky part of the model proposed by Erlebacher et al. [17] for compressible flows. The subgrid-scale viscous stress tensor in Eq. (3) is defined here as

$$\tau_{ij} = \mu_t(2\tilde{S}_{ij} - \tfrac{2}{3}\tilde{S}_{mm}\delta_{ij}) - \tfrac{2}{3}\bar{\rho}k^{\mathrm{SGS}}\delta_{ij} \tag{5}$$

where k^{SGS} is the subgrid kinetic energy

$$k^{\mathrm{SGS}} = C_I\Delta^2\tilde{S}_{mn}\tilde{S}_{mn} \tag{6}$$

μ_t is the subgrid-scale dynamic viscosity

$$\mu_t = C_R\bar{\rho}\Delta^2\sqrt{\tilde{S}_{mn}\tilde{S}_{mn}} \tag{7}$$

and $\tilde{S}_{ij}$ is the Favre-filtered strain rate tensor given by

Table 1 Normalized nominal impedance for the frequencies considered in case I and case II, from Jones et al. [15]

f, Hz	$R/(\rho_\infty c_\infty)$	$X/(\rho_\infty c_\infty)$	$R_{\mathrm{exit}}/(\rho_\infty c_\infty)$	$X_{\mathrm{exit}}/(\rho_\infty c_\infty)$
500	0.62	−1.66	0.850	−0.133
1000	0.48	0.03	1.090	0.275
1500	1.09	1.23	0.855	−0.169
2000	4.38	0.88	1.035	0.235
2500	1.50	−1.55	1.003	−0.199
3000	0.72	−0.30	0.947	0.162

Table 2 Flow properties

	p_0, Pa	T_0, K	M_{avg}	ρ_∞, kg/m^3	c_∞, m/s
Case I	101,954	296.2	0.000	1.199	344.99
Case II	114,386	295.9	0.335	1.245	339.45

Table 3 Legend for Figs. 2–7. Note that, for all simulations, the experimentally measured 2-D flow profile at axial position 0.2032 m from the inlet has been imposed as the inlet boundary condition

Method	Character
LES with free slip on walls	Black solid line
LNSE based on high-Re RANS steady-state solution with wall function	Red dashed line
LNSE based on high-Re RANS steady-state solution with free slip on walls	Red dash-dotted line
LNSE based on low-Re RANS steady-state solution with no slip on walls	Blue dashed line
Linearized Euler based on high-Re RANS steady-state solution with wall functions	Green dashed line
Experimental data	Black circles

$$\tilde{S}_{ij} = \frac{1}{2}\left(\frac{\partial \tilde{u}_i}{\partial x_j} + \frac{\partial \tilde{u}_j}{\partial x_i}\right) \tag{8}$$

The filter width used in Eqs. (6) and (7) is the minima of the local grid cell, that is, $\Delta = \min(\Delta_1, \Delta_2, \Delta_3)$. The Smagorinsky model constants C_R and C_I, where the latter is a compressibility correction constant, are here given by

$$C_R = 0.012 \qquad C_I = 0.0066 \tag{9}$$

The system of governing equations are closed by two assumptions of the thermodynamics of gas. First, the gas is considered thermally perfect, meaning that it obeys the gas law. Second, that the gas is calorically perfect, implying that internal energy and enthalpy are linear functions of temperature.

B. Linearized Navier–Stokes Equations Method

1. Average Solver

The linearized Navier–Stokes equations require an average flowfield in which the perturbations can propagate. As solver for the average flowfield, the commercial software CFX 10.0 was used. The compressible formulation of the Reynolds-averaged Navier–Stokes equations (RANS) with the k-ω shear stress transport model was solved to acquire the average flows. The conservative flow variables ($\overline{\rho}, \overline{\rho u}, \overline{\rho v}, \overline{\rho w}, \overline{\rho e_0}, \overline{\rho k}, \overline{\rho \varepsilon}$) as well as the dynamic viscosity μ were stored from the average flow and used as a reference solution in the LNSE solver.

2. Linearized Solver

The solver used for the computational aeroacoustics simulations is based on a frequency-domain formulation of the linearized Navier–Stokes equations and result from a linearization of the unsteady RANS equations. The difference between the actual flow state and a time-averaged flow state may be denoted by the perturbations $\mathbf{Q}'$. If the perturbations are assumed to vary harmonically in time, a perturbation state vector can be defined as

$$\mathbf{Q}' = \sum_{n=-\infty}^{\infty} \hat{\mathbf{Q}}_n e^{i\omega_n t} \tag{10}$$

where $\hat{\mathbf{Q}}_n$ is the complex flow state vector for the harmonic frequency ω_n. Assuming linear perturbations, the LNSE equations valid in the frequency domain for nth frequency can then be written as

$$i\omega_n \hat{\mathbf{Q}}_n + \frac{\partial}{\partial x_j}(\mathcal{F}_{0j}\hat{\mathbf{Q}}_n) = 0 \tag{11}$$

where

$$\mathcal{F}_{0j} = \left(\frac{\partial \mathcal{F}_j}{\partial \mathbf{Q}}\right)_0 \tag{12}$$

The subscript 0 refers to the reference solution, that is, the average flow state vector $\mathbf{Q}_0$ obtained from the average flow solver. The turbulence quantities are not included in the perturbed state vector, but the average turbulence quantities define a frozen turbulent-eddy viscosity field in the reference solution. See Stridh [18] and Billson [19] for more information.

IV. Acoustic Liner Boundary Condition

A. Frequency Domain

The impedance boundary condition implemented in the linearized Navier–Stokes equations solver is

$$Z = \frac{\hat{p}}{\hat{v}_n} = R + iX \tag{13}$$

where $\hat{p}$ and $\hat{v}_n$ are the wall pressure and wall normal velocity, respectively. R is the liner resistance and X is the liner reactance. The pressure perturbation in the cell closest to the wall is used as an approximation of the wall pressure. The wall normal velocity $\hat{v}_n$ is then computed as $\hat{v}_n = \hat{p}/Z$.

B. Time Domain

As the impedance is a complex number, see Eq. (13), it cannot be directly implemented as a boundary condition in time-domain simulations. For this, the broadband time-domain impedance boundary condition (BTDIBC) proposed by Tam and Auriault [5] has been used. This models a mass-spring-damper system similar to a Helmholtz resonator and is given by

$$\frac{\partial p}{\partial t} = R_0 \frac{\partial v_n}{\partial t} - X_- v_n + X_+ \frac{\partial^2 v_n}{\partial t^2} \tag{14}$$

The two-way coupling between the acoustic liner and the domain is made via the wall normal velocity and the time derivative of the pressure, where the sound wave is responsible for the latter and the liner reacts by introducing a wall normal velocity. Consistent with the energy equation in Eqs. (1–3), the pressure can be expressed in terms of conservative variables as

$$p = (\gamma - 1)\left[\rho e_0 - \tfrac{1}{2\rho}(\rho u_i)(\rho u_i)\right] \tag{15}$$

from which the time derivative of the pressure is easily obtained

$$\frac{\partial p}{\partial t} = (\gamma - 1)\left(\frac{\partial(\rho e_0)}{\partial t} + \frac{1}{2\rho^2}\frac{\partial \rho}{\partial t}(\rho u_i)(\rho u_i) - \frac{1}{\rho}(\rho u_i)\frac{\partial(\rho u_i)}{\partial t}\right) \tag{16}$$

where the right-hand side is expressed in conservative variables only. As the temporal derivatives of the conservative variables are calculated from Eq. (1), Eq. (16) is unambiguous at each time step. Because the BTDIBC contains a second time derivative of the wall normal velocity, the boundary condition needs to be rewritten as a system of first-order differential equations for implementation purposes:

$$\frac{\partial}{\partial t}\begin{bmatrix} v_n \\ \Phi \end{bmatrix} = \begin{bmatrix} \Phi \\ \frac{1}{X_+}\left(\frac{\partial p}{\partial t} - R_0\Phi + X_- v_n\right) \end{bmatrix} \tag{17}$$

This system of equations is added into the original Runge–Kutta time-step cycle. The BTDIBC, based on a single set of parameters, could possibly be applied to the lower frequency range, up to the first

resonance frequency, for any single degree of freedom liner. However, the resistance and reactance of the tested liner cannot be represented by one set of impedance constants for the entire frequency range. Because the frequency of the incoming sound wave is known, the constants have been set for each simulation to give the correct impedance for the given frequency.

V. Computational Method

A. Numerical Scheme

The solvers used for the LES and LNSE simulations are codes in the G3D family of finite volume method codes developed by Eriksson [20]. These codes solve the compressible flow equations in conservative form on a boundary-fitted, curvilinear nonorthogonal multiblock mesh. In the LES, the Favre-filtered Navier–Stokes equations were solved using a finite volume method with a low-dissipation third-order upwind-biased scheme for the convective fluxes and a second-order centered difference approach for the diffusive fluxes. The temporal derivatives were calculated using a second-order three-stage Runge–Kutta technique. To enable simulations with a large number of degrees of freedom, routines have been implemented for parallel computations using MPI (message passing interface) libraries. Detailed descriptions of the numerical scheme and boundary conditions are given in Eriksson [20], Billson [19], and Andersson [12]. In the LNSE solver, Eq. (11) is solved iteratively by introducing a pseudotime and using Runge–Kutta time stepping. To accelerate the convergence to steady state, a local time step is used. In the local time stepping, the time step in each cell is maximized to correspond to a certain Courant–Friedrichs–Lewy (CFL) number, say CFL = 0.8, based on a local spectral radius. When the normalized impedance of the wall is less than unity (normalized by $\rho_\infty c_\infty$), the local time step should be changed to match the new spectral radius accounting for the wall impedance. This is done by reducing the local time step by the ratio between the wall impedance and the air impedance [see Eqn. (18)]:

$$\Delta t_{\text{red}} = \Delta t \cdot \min[1, \text{amp}(Z)/(\rho_\infty c_\infty)] \tag{18}$$

B. Computational Setup

1. Large-Eddy Simulation Method

The computational domain is discretized using a block-structured boundary-fitted mesh consisting of $296 \times 34 \times 34$ cells giving an axial equidistant section representing the GIT duct with resolution to resolve a 3000 Hz sound wave by approximately 40 cells. To this domain, a second part, consisting of $49 \times 34 \times 34$ cells, is added which is axially stretched and extends an additional duct length downstream. At the inlet, a flow profile is used based on the 0.2032 m Mach number profile given from the experiment; relative location in the GIT is depicted as a shaded surface in Fig. 1. Absorbing boundary conditions are used on the inlet and outlet boundaries and free-slip wall condition for all walls. For the liner wall, the BTDIBC is used (see Sec. IV.B). The reason for using a free-slip wall condition instead of a no-slip condition is due to the difficulty in reproducing the experimental flow environment. However, in case II, the y^+ was found to be in the range of 60–100 which makes it valid for wall functions. This will be discussed in Sec. VI.B.1.

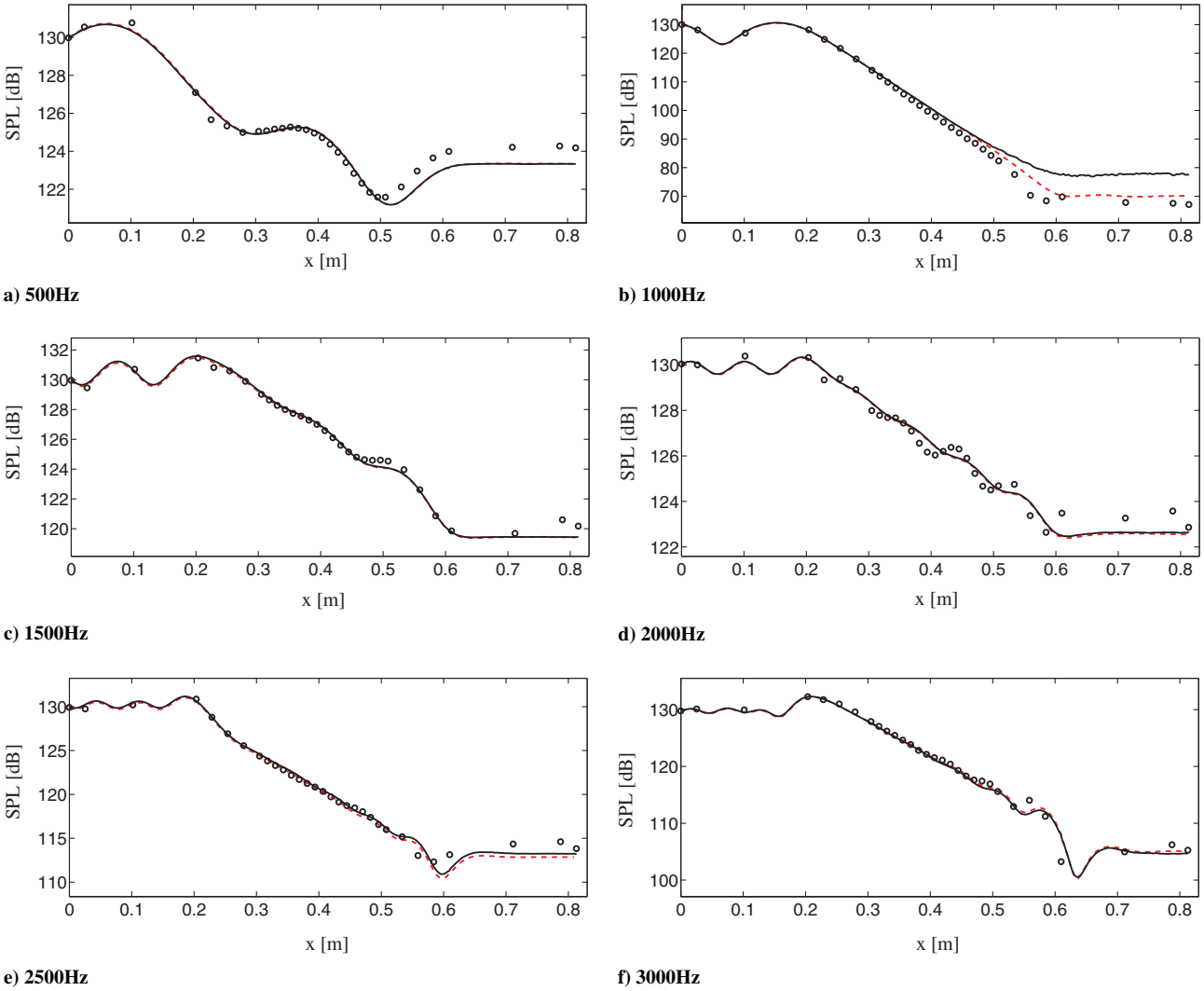

Fig. 2 SPL results for case I. For legend, see Table 3.

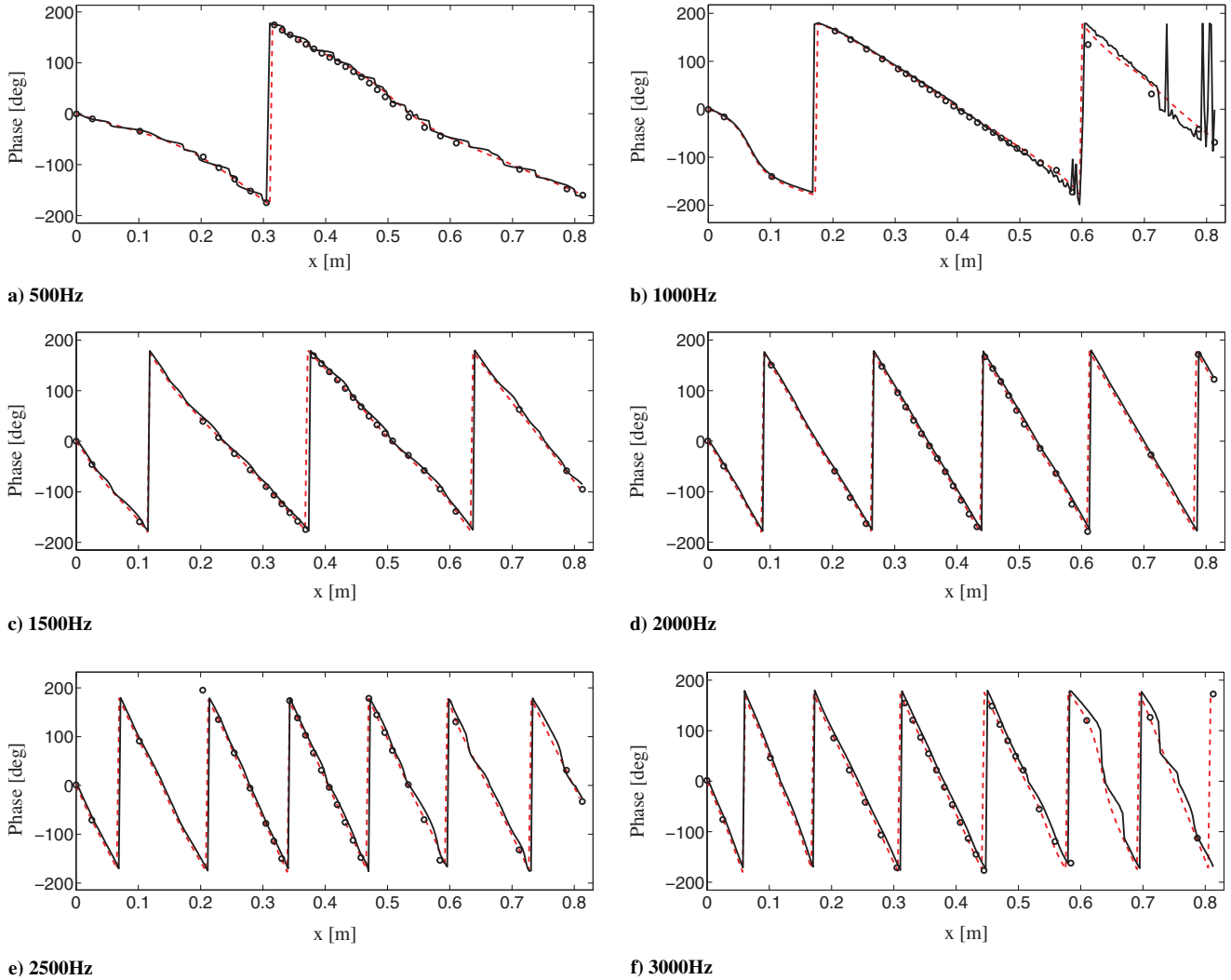

Fig. 3 Phase results for case I. For legend, see Table 3.

2. Linearized Navier–Stokes Equations Method

The computational domain for the LNSE simulations is discretized using two different grids. The coarse grid consist of $296 \times 34 \times 34$ cells, which gives a y^+ of about 160 in the liner section. The finer grid is a low-Re grid with $296 \times 76 \times 76$ cells, giving a y^+ of one. The axial resolution in both grids ensured 40 cells per wavelength in the axial direction for a 3000 Hz sound wave. The inlet boundary conditions for the average flowfield are based on total pressure and total temperature profiles. The profiles are given by the Mach number profile from the experiment at 0.2032 m into the test section. The outlet boundary condition is based on static pressure and is adjusted to get the same average Mach number $M = 0.335$ as in the experiments. The inlet and outlet boundary conditions for the LNSE are 1-D absorbing boundary conditions based on characteristic variables. The duct exit impedance given from the experiments are used at the outlet boundary to simulate the duct exit reflection [15] (see Table 1). The wall boundary condition for the coarse grid is based on wall functions, and the finer grid is a resolved wall boundary. Also, for the coarse grid, a case with a free-slip wall boundary condition is computed.

VI. Results

A. Case I: $M_{\text{avg}} = 0.000$

In this section, the results for case I (zero Mach number) will be presented. Overall, the results using the LES method and the LNSE method are in very good agreement with experimental data (see Figs. 2 and 3). The leveling in the 1000 Hz case for the LES method is the result of using single precision. The phase diagrams are on target against experimental data, except for some deviation in the LES case. The fluttering that can be noticed in the 1000 Hz case at the end part of the duct is linked with the single precision data handling. The reason for not using double precision is that the aim of the LES method is to use it in large computations where computer resources are limited. The results for this case validate the implementation of the methods presented in this paper for no-flow cases.

B. Case II: $M_{\text{avg}} = 0.335$

Case II is a more demanding case that involves the effects of a grazing flow over the liner. This section is divided into two parts dealing with the representation of the flowfield and the acoustic results, respectively.

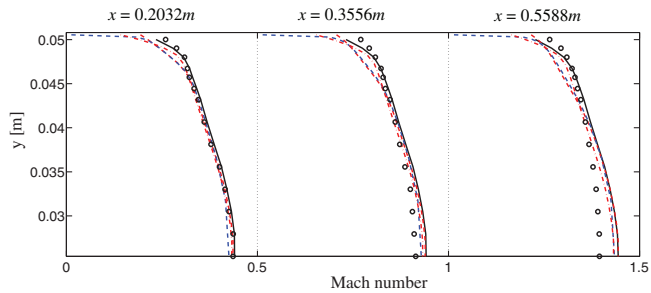

Fig. 4 Comparison of Mach profiles at axial positions at midspan of the channel. Plotted from midheight of the channel up to the liner wall. Profiles staggered with increment of Mach 0.5 per axial position. For legend, see Table 3.

1. *Representation of the Flowfield*

From the experiment, 2-D profiles of Mach number were given at three axial positions, located at 0.2032, 0.3556, and 0.5588 m from the inlet. The downstream development of the flow in the experiment is tending toward a flatter profile (see Fig. 4). Attempts were made to get the same flow development in the numerical simulations (LES and RANS), but they were all unsuccessful. The reason behind the deviation between the measured and numerically predicted mean-flow profiles cannot be determined without additional measurement data. To get mean profiles as close to the experiment as possible, the 0.2032 m experimental Mach number profile was imposed as the inlet boundary condition in the simulations. In the LES simulations, a free-slip wall boundary condition was used to retain the 0.2032 m flow profile throughout the channel and to stay as close to the experiment as possible. In the LNSE simulations, both free-slip and no-slip wall boundary conditions were used. Figure 4 shows Mach number profiles from the experiment and simulations compared at midspan at the three axial positions where experimental data are available. It is evident that the downstream evolution in the simulations differs from the experiment. Including wall friction in the simulations gives a growth in boundary-layer thickness downstream which, in turn, leads to an increase of the centerline velocity, which is opposite to the downstream development of the flow in the experiment.

2. *Flow Instability*

In the LES and the low-*Re* LNSE simulations, a hydrodynamic instability was found in the 1000 Hz case that was not captured in the high-*Re* LNSE simulations (see Fig. 5). The instability appears at the leading edge of the liner and continues to grow downstream. Downstream of the trailing edge of the liner, the instability ceases to grow and is merely convected to the outlet. The numerical results where the hydrodynamic instability appeared are in good agreement with the experiment. The simulations where it did not appear deviated more from the experiments close to the end of the liner and downstream to the duct exit. The hydrodynamic instability is clearly physical and was a part of the experimental results as well. The reason that it did not appear in the high-*Re* LNSE simulations is unclear, but may be due to the shape of the boundary layer closest to

a) LNSE based on a high-Re RANS base flow solution

b) LNSE based on a low-Re RANS base flow solution

Fig. 5 Pressure fluctuation contour plots. Slices taken at midspan over the lined section.

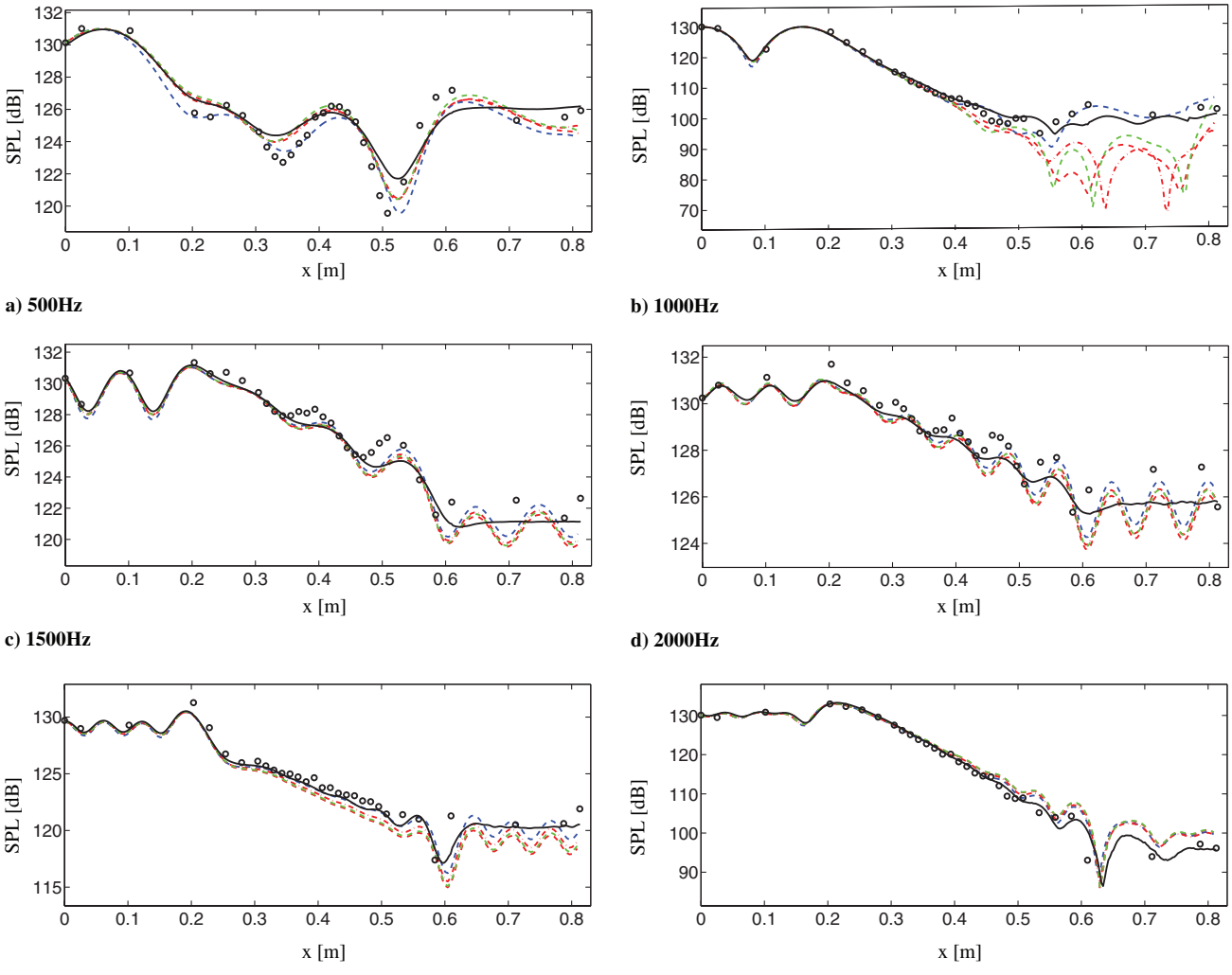

a) 500Hz

b) 1000Hz

c) 1500Hz

d) 2000Hz

e) 2500Hz

f) 3000Hz

Fig. 6 SPL results for case II. For legend, see Table 3.

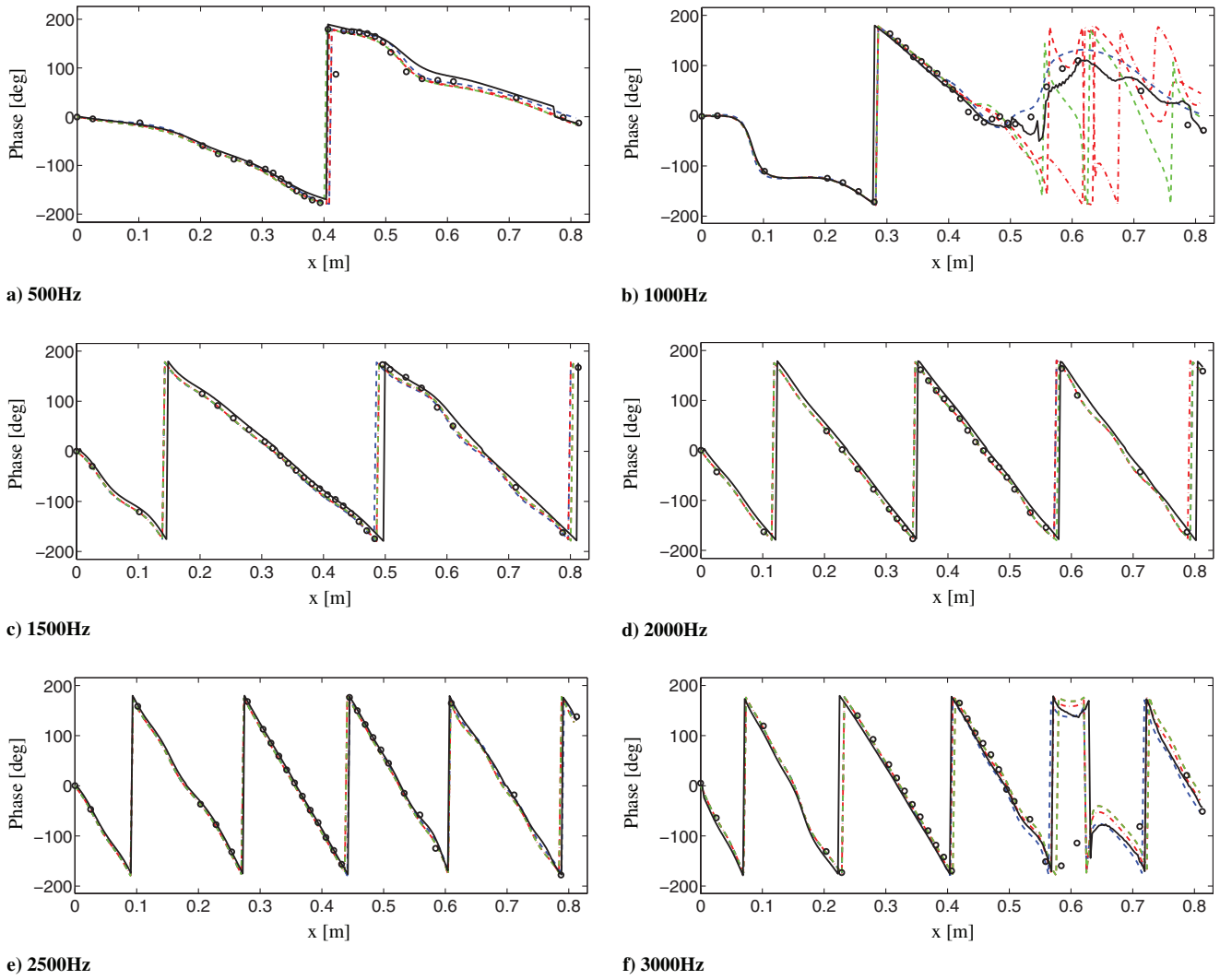

Fig. 7 Phase results for case II. For legend, see Table 3.

the liner wall. This instability has previously been reported by Li et al. [11], who interpreted it to be a Tollmien–Schlichting instability. However, this characterization of the phenomena seems, in our opinion, to be rather doubtful and therefore we prefer to just use the term hydrodynamic instability.

3. Opposite Liner Wall Sound Pressure Level and Phase Results

Numerical results are presented against experimental data in Figs. 6 and 7. The overall impression of the results is that the methods are capable of predicting the effect of the liner very well. A general difference between the time- and frequency-domain methods is that the frequency-domain method responds better to small-scale spatial sound pressure level (SPL) variations. However, both methods successfully predict the SPL at the end of the liner for all frequencies. All LNSE configurations give the same quantitative result except in the 1000 Hz case. This is the effect of the hydrodynamic instability which is not captured in the high-*Re* LNSE simulations (see Sec. VI.B.1). Considering the phase, both methods give the same result and are in very good agreement with experimental data. The effect of the hydrodynamic instability is apparent in the 1000 Hz case where the predictions diverge from the experimental data for the high-*Re* LNSE cases. For the low-*Re* LNSE and LES cases, the correct phase relation is captured and so is the effect of the hydrodynamic instability.

VII. Conclusions

This paper demonstrates the validity of using nominal impedance as a boundary condition for modeling an acoustic liner in both the time- and frequency-domain. This is shown using both time-domain LES and frequency-domain LNSE. Two grids were used to assess the effect of the wall resolution on the acoustic response from the impedance boundary condition. The two cases that performed best in predicting the correct liner effect were the LES and the LNSE based on a resolved low-*Re* RANS steady-state flowfield. Arguments could be made that the boundary layer is fully resolved when using a low-*Re* LNSE model and thereby the use of nominal impedance is obvious. However, when comparing the flow profiles from the simulations with the experimental data there are quite large differences, especially close to the wall. Even the low-resolution, high-*Re* LNSE simulations performed well in all cases except in one case where there was a hydrodynamic instability over the lined section of the duct. The exact details close to the wall seem to be of secondary importance as long as the large-scale mean-flow refraction is resolved. The mean-flow effect on the wall impedance is then handled by the equations and the nominal impedance may be used. This greatly simplifies the modeling of acoustically treated walls. The type of acoustic liner studied in the present test case is very linear, and the authors see a need for further validation of the methods against more conventional liners.

Acknowledgments

The authors thank Michael G. Jones for providing the database of measurements of the NASA Grazing Incidence Tube. Financial support for the first author by Swedish Defence Material Administration Contract no. 217046-LB739715 is acknowledged. The large-

eddy simulations computations were performed on C3SE computing resources.

References

[1] Ingard, U., "Influence of Fluid Motion Past a Plane Boundary on Sound Reflection, Absorption, and Transmission," *Journal of the Acoustical Society of America*, Vol. 31, No. 7, 1959, pp. 1035–1036. doi:10.1121/1.1907805

[2] Myers, M. K., "On the Acoustic Boundary Condition in the Presence of Flow," *Journal of Sound and Vibration*, Vol. 71, No. 3, 1980, pp. 429–434. doi:10.1016/0022-460X(80)90424-1

[3] Tester, B. J., "The Propagation and Attenuation of Sound in Lined Ducts Containing Uniform or Plug Flow," *Journal of Sound and Vibration*, Vol. 28, No. 2, 1973, pp. 151–203. doi:10.1016/S0022-460X(73)80102-6

[4] Rienstra, S. W., "A Classification of Duct Modes Based on Surface Waves," *Wave Motion*, Vol. 37, No. 2, 2003, pp. 119–135. doi:10.1016/S0165-2125(02)00052-5

[5] Tam, C. K. W., and Auriault, L., "Time-Domain Impedance Boundary Conditions for Computational Aeroacoustics," *AIAA Journal*, Vol. 34, No. 5, 1996, pp. 917–923. doi:10.2514/3.13168

[6] Özyörük, Y., and Long, L. N., "Time-Domain Calculation of Sound Propagation in Lined Ducts with Sheared Flows," *AIAA Journal*, Vol. 38, No. 5, 2000, pp. 768–773. doi:10.2514/2.1056

[7] Fung, K.-Y., and Ju, H., "Broadband Time-Domain Impedance Models," *AIAA Journal*, Vol. 39, No. 8, 2001, pp. 1449–1454. doi:10.2514/2.1495

[8] Ju, H., and Fung, K.-Y., "Time-Domain Impedance Boundary Conditions with Mean Flow Effects," *AIAA Journal*, Vol. 39, No. 9, 2001, pp. 1683–1690. doi:10.2514/2.1525

[9] Özyörük, Y., Long, L. N., and Jones, M. G., "Time-Domain Numerical Simulation of a Flow-Impedance Tube," *Journal of Computational Physics*, Vol. 146, No. 1, 1998, pp. 29–57. doi:10.1006/jcph.1998.5919

[10] Li, X. D., and Thiele, F., "Numerical Computation of Sound Propagation in Lined Ducts by Time-Domain Impedance Boundary Conditions," AIAA Paper 2004-2902, 2004.

[11] Li, X. D., Richter, C., and Thiele, F., "Time-Domain Impedance Boundary Conditions for Surfaces with Subsonic Mean Flows," *Journal of the Acoustical Society of America*, Vol. 119, No. 5, 2006, pp. 2665–2676. doi:10.1121/1.2191610

[12] Andersson, N., "A Study of Subsonic Turbulent Jets and Their Radiated Sound Using Large-Eddy Simulation," Ph.D. Thesis, Div. of Fluid Dynamics, Chalmers Univ. of Technology, Gothenburg, Sweden, 2005, ISBN 91-7291-679-6.

[13] Stridh, M., and Eriksson, L.-E., "Modeling Unsteady Flow Effects in a 3D Transonic Compressor," American Society of Mechanical Engineers GT2005-68149, 2005.

[14] Zheng, S., and Zhuang, M., "Verification and Validation of Time-Domain Impedance Boundary Condition in Lined Ducts," *AIAA Journal*, Vol. 43, No. 2, 2005, pp. 306–313. doi:10.2514/1.7214

[15] Jones, M. G., Watson, W. R., and Parrott, T. L., "Benchmark Data for Evaluation of Aeroacoustic Propagation Codes with Grazing Flow," AIAA Paper 2005-2853, 2005.

[16] Parrott, T. L., Watson, W. R., and Jones, M. G., "Experimental Validation of a Two-Dimensional Shear-Flow Model for Determining Acoustic Impedance," NASA TP-2679, 1987.

[17] Erlebacher, G., Hussaini, M. Y., Speziale, C. G., and Zang, T. A., "Toward the Large-Eddy Simulation of Compressible Turbulent Flows," *Journal of Fluid Mechanics*, Vol. 238, No. 1, 1992, pp. 155–185. doi:10.1017/S0022112092001678

[18] Stridh, M., "Modeling Unsteady Flow Effects in 3D Throughflow Calculations," Ph.D. Thesis, Div. of Fluid Dynamics, Chalmers Univ. of Technology, Gothenburg, Sweden, 2006, ISBN 91-7291-775-X.

[19] Billson, M., "Computational Techniques for Turbulence Generated Noise," Ph.D. Thesis, Div. of Thermo and Fluid Dynamics, Chalmers Univ. of Technology, Gothenburg, Sweden, 2004, ISBN 91-7291-423-8.

[20] Eriksson, L.-E., "Development and Validation of Highly Modular Flow Solver Versions in G2DFLOW and G3DFLOW," Volvo Aero Corp., Internal Rept. 9970-1162, 1995.

C. Bailly
Associate Editor